Some Effects of Model Resolution on Simulated Gravity Waves Generated by Deep, Mesoscale Convection

TODD P. LANE AND JASON C. KNIEVEL

National Center for Atmospheric Research, Boulder, Colorado*

(Manuscript received 17 March 2004, in final form 2 November 2004)

ABSTRACT

Over the past decade, numerous numerical modeling studies have shown that deep convective clouds can produce gravity waves that induce a significant vertical flux of horizontal momentum. Such studies used models with horizontal grid spacings of O(1 km) and produced strong gravity waves with horizontal wavelengths greater than about 20 km. This paper is an examination of how simulated gravity waves and their momentum flux are sensitive to model resolution. It is shown that increases in horizontal resolution produce more power in waves with shorter horizontal wavelengths. This change in the gravity waves' spectra influences their vertical propagation. In some cases, gravity waves that were vertically propagating in coarse simulations become vertically trapped in fine simulations, which strongly influences the vertical flux of horizontal momentum.

1. Introduction

Gravity waves generated by deep convective clouds play an important role in the momentum budget of the middle atmosphere (Fritts and Alexander 2003). In general, these gravity waves can be separated into two scales: *short* gravity waves generated by individual convective systems and cells on the meso-β and meso-γ scales (e.g., squall lines, supercells, deep cumuli, and individual updrafts within those systems and cells), and *long* gravity waves and inertia–gravity waves generated by clusters or complexes of clouds on the meso-α and synoptic scales. This paper focuses on those *short* waves generated by squall lines and the structures that compose squall lines.

The study of short convectively generated gravity waves has blossomed over the past decade, with observational studies (e.g., Pfister et al. 1993; Alexander et al. 2000), analytic studies (e.g., Holton et al. 2002), and numerical modeling at the cloud-resolving scale in both two dimensions (e.g., Fovell et al. 1992; Beres et al. 2002; Song et al. 2003) and three dimensions (e.g., Piani et al. 2000). Modeling studies have proven particularly valuable because of their clearer and more complete picture of the wave structure and the dynamics underlying wave excitation. Simulations in such studies have been used to estimate how drag from convectively generated gravity waves contributes to forcing the quasi-biennial oscillation (QBO) (e.g., Alexander and Holton 1997; Piani et al. 2000). Simulations have also contributed to the development of gravity wave drag parameterizations, either through providing the theoretical basis for that parameterization or by constraining or defining the values of tunable parameters within those parameterizations (e.g., Kershaw 1995; Beres et al. 2004). Thus, it is important to ensure that the properties of gravity waves produced by cloud-resolving models are realistic.

The use and effectiveness of cloud-resolving models for studying convectively generated gravity waves has been hampered somewhat by computer power. Early studies such as that by Fovell et al. (1992) used 1.5-km horizontal grid spacing in a two-dimensional model. More recently, increased computer power allowed similar grid spacings in three-dimensional models (e.g., Piani et al. 2000) and a much higher grid spacing (50 m) in two dimensions (Lane et al. 2003). Nevertheless, most recent studies retained O(1 km) horizontal grid

* The National Center for Atmospheric Research is sponsored by the National Science Foundation.

Corresponding author address: Todd Lane, School of Earth Sciences, The University of Melbourne, Melbourne, Victoria 3010, Australia.
E-mail: t.lane@earthsci.unimelb.edu.au

spacing to allow the use of three dimensions, larger two-dimensional domains, or more model realizations under different flow conditions. This is also the case in studies of convective systems and their organization. However, Bryan et al. (2003) questioned the use of $O(1\text{ km})$ as the *standard* grid spacing in cloud-resolving models and showed that this spacing does not permit full representation of the details of convective clouds, including the horizontal scales of their updrafts. It seems likely that horizontal grid spacing also influences the properties of gravity waves generated by deep convection. For example, using a model with 1-km horizontal grid spacing, Lane and Reeder (2001) identified a strong wave response at horizontal wavelengths of ~20 km; then, using a model with 50-m grid spacing, Lane et al. (2003) identified a strong wave response at horizontal wavelengths of ~5 km. Not only did the gravity waves in these studies have different wavelengths and propagation characteristics, but the waves with 5-km wavelengths identified by Lane et al. (2003) simply cannot be properly resolved by grid spacings of $O(1\text{ km})$. Although previous studies have resolved gravity waves sufficiently well in the vertical dimension, the same cannot be said for the horizontal dimension.

The purpose of this paper is to examine the sensitivity of simulated, convectively generated gravity waves to horizontal grid spacing. Accordingly, we address the following questions. How do gravity wave spectra change with horizontal resolution? How does this change affect wave propagation? What horizontal grid spacing is sufficient to robustly represent gravity wave spectra? How does resolution affect the wave-induced, vertical flux of horizontal momentum? To answer these questions, we systematically adjusted the horizontal grid spacing in a series of model simulations. We also tested our results' sensitivity to the background sounding, vertical resolution, and the primary numerical model used.

2. Numerical models and configurations

Two numerical models were used for this study. The Clark–Hall Model (CHM; Clark 1977; Clark et al. 1996) was used for the majority of the numerical experiments. It is an anelastic, nonhydrostatic model with a second-order finite-difference scheme, sixth-order spatial filtering, and a first-order (Smagorinsky) subgrid closure. The CHM has been used in a number of studies of convectively generated gravity waves. We compared results from the CHM to those from version 1.3 of the Weather Research and Forecasting (WRF) Model (Skamarock et al. 2001; Wicker and Skamarock 2002). The WRF Model is very different from the CHM, and these differences are a rigorous test of our results' sensitivity to the choice of model. The WRF Model is compressible, and it employs time-split advection that is third-order accurate, implicit filtering, and a 1.5-order subgrid TKE scheme. The CHM uses a combination of the Kessler (1969) warm rain parameterization and the Koenig–Murray (1976) ice parameterization; the WRF Model uses a modified version of the Lin et al. (1983) microphysics parameterization. In all cases, the earth's rotation, surface friction, and absorption and scattering of radiation were neglected.

To allow numerous simulations to be completed, we restricted our focus to two dimensions. Domains are 500 km wide and 40 km high with a Rayleigh-friction absorber in the top 14 km. Horizontal grid spacings (ΔX) are 2 km, 1.5 km, 1 km, 750 m, 500 m, 250 m, 125 m, and 62.5 m. Unless otherwise noted, the simulations with horizontal grid spacings greater than or equal to 500 m have 200-m vertical grid spacing (ΔZ). The simulations with 250-, 125-, and 62.5-m horizontal grid spacing have vertical grid spacings of 100, 100, and 62.5 m, respectively. Therefore, the effect of vertical resolution is not exactly isolated from our set of simulations, because the simulations with highest horizontal resolution have finer vertical grid spacing than do the coarser simulations. However, it will be shown later in the paper that the simulation results at coarse resolution are relatively insensitive to vertical resolution.

We used two initial soundings. The first was the Weisman and Klemp (1982) analytic sounding (WK) with a wind speed that increased linearly from -12 m s^{-1} at the surface to 0 m s^{-1} at 2.5 km AGL. Wind was unsheared above 2.5 km AGL. The WK sounding has been employed in numerous studies of gravity waves (e.g., Fovell et al. 1992; Song et al. 2003). The second sounding (BIS) was a modified version of that taken at 0000 UTC 11 July 1997 above Bismarck, North Dakota—the same sounding used by Lane et al. (2003) in their two-dimensional experiments (see their Figs. 3 and 4). This second sounding enabled us to evaluate the behavior of gravity waves in flow with realistic wind shear above cloud top. The CHM was initialized with both the WK and BIS soundings, using all of the horizontal grid spacings mentioned above. The WRF Model was initialized with the WK sounding, using a subset of the grid spacings.

In all experiments, convection was triggered with a 2-K potential temperature perturbation that was 10 km wide, 2 km deep, and was centered at the middle of the model domain at the surface. In all cases, this initial perturbation was sufficient to initiate a squall line that was long-lived. The primary results presented herein are insensitive to the method of storm initialization; test

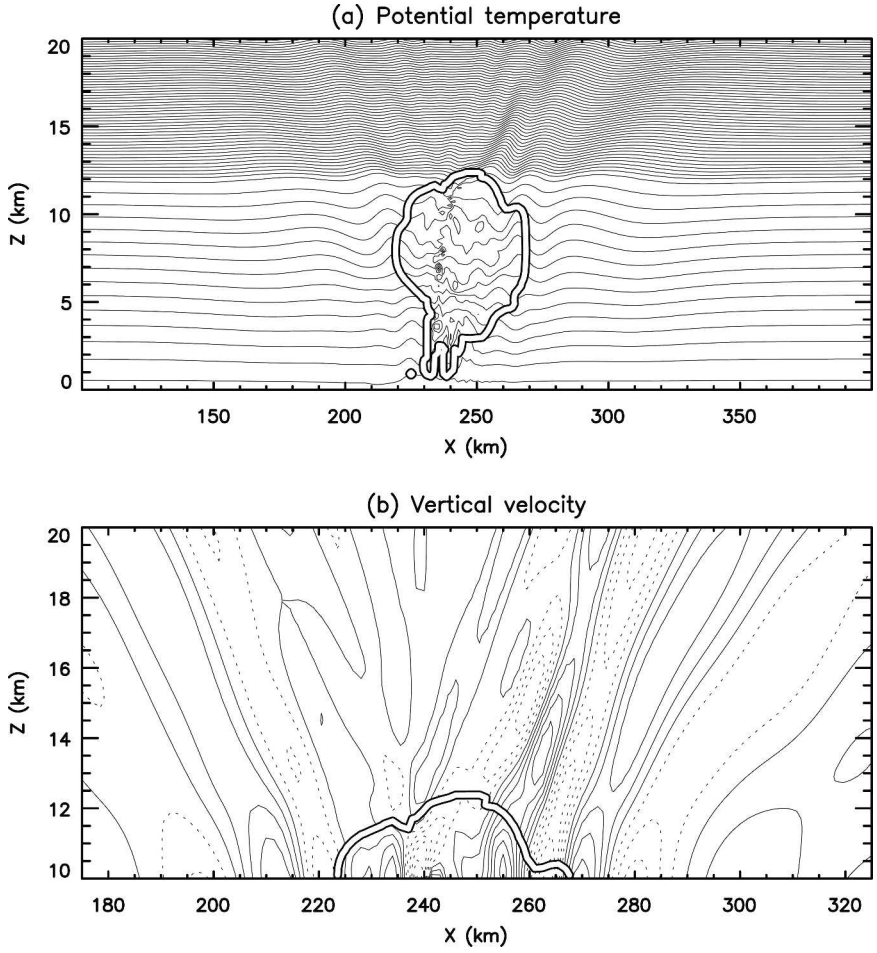

FIG. 1. Contours of (a) potential temperature at intervals of 3 K and (b) vertical velocity at intervals of 0.5 m s^{-1} 60 min into a simulation by the CHM initialized with the WK sounding, with $\Delta X = 1.5$ km and $\Delta Z = 200$ m. In both (a) and (b), the black-edged white line is the cloud water mixing ratio contour of 0.05 g kg^{-1}. In (b) negative vertical velocity contours are dashed.

simulations were initialized with a local surface heating, which allowed convection to evolve more slowly, starting from a scale that was effectively "chosen" by the model. These simulations produced qualitatively similar results to those initialized with the bubble.

3. Results

a. Unsheared flow in the upper troposphere

After initialization, each simulation was integrated for 3 h. For each background sounding, the simulations at different resolutions produce convection with similar timing and overall cloud structure. There are, however, consistent differences.

The first difference is that the horizontal scale of the updrafts within the clouds shrinks significantly as the horizontal grid spacing decreases. This can be seen in the deformation of the isentropes at 60 min in simulations by the CHM at $\Delta X = 1.5$ km and $\Delta X = 62.5$ m, initialized with the WK sounding (Figs. 1a and 2a). Not surprisingly, the isentropes are relatively smooth in the coarse simulation but have much more structure in the fine simulation. Further investigation of these changes is beyond the scope of this study. The topic was examined in detail for three dimensions by Bryan et al. (2003).

The second important difference is the horizontal scale of the gravity waves. Like the updraft scale, the horizontal wavelength of the gravity waves above the clouds shrinks significantly with the horizontal grid spacing. This reduction in wavelength can be seen in Figs. 1b and 2b. Visual inspection reveals that the simulation with $\Delta X = 1.5$ km has strong gravity waves with horizontal wavelengths that are ~20 km or greater, whereas the simulation with $\Delta X = 62.5$ m has strong gravity waves with horizontal wavelengths that are ~5

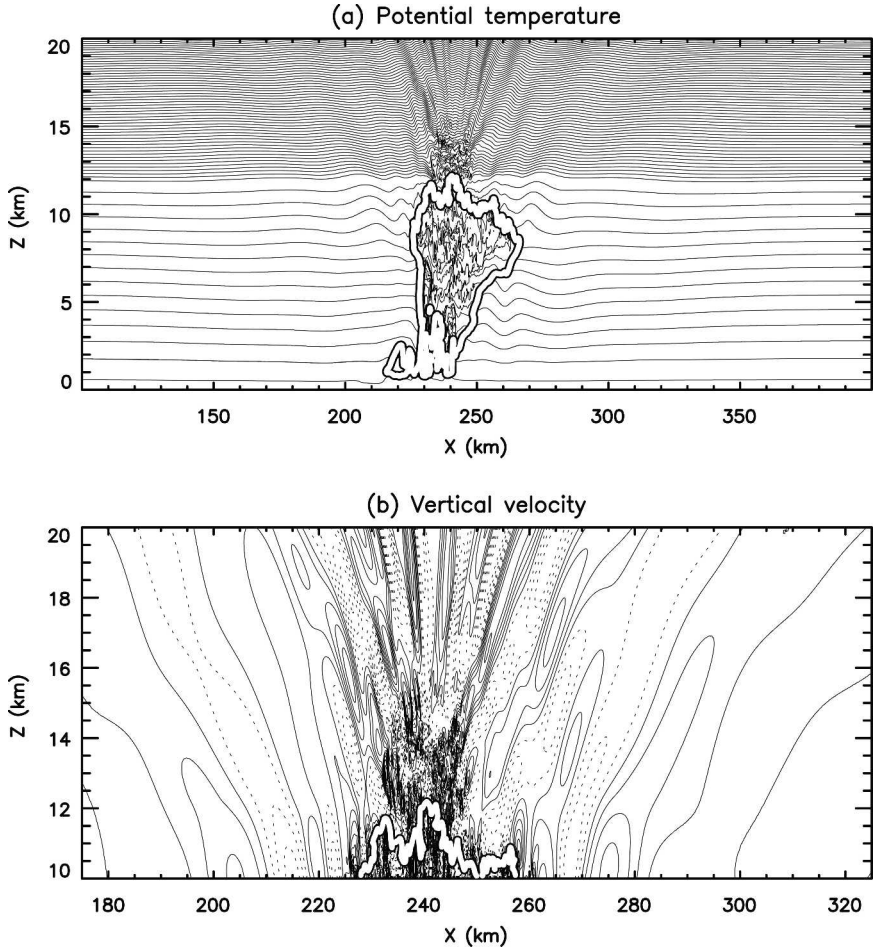

FIG. 2. Same as Fig. 1 except for a simulation with $\Delta X = 62.5$ m and $\Delta Z = 62.5$ m.

km or greater. The phase lines of the gravity waves in the 62.5-m simulation are steeper than those in the 1.5-km simulation; this change in the slope of the phase lines implies a change in the vertical propagation characteristics of the gravity waves. Finally, the amplitudes of the gravity waves at higher resolution are larger.

The above results suggest that the simulation with $\Delta X = 1.5$ km has not reached numerical convergence and is in a regime in which numerical effects constrain the dynamics. Later in the paper we spectrally analyze the simulations in an attempt to determine when properties of the gravity waves have converged.

To test the sensitivity of the simulated waves to vertical resolution, we integrated the CHM with $\Delta X = 1.5$ km and $\Delta Z = 400$ m. Figure 3a shows vertical velocity from this simulation, which can be directly compared to the case with half the vertical grid spacing shown in Fig. 1b. There are negligible differences between these two cases, suggesting that 200-m vertical grid spacing is sufficient to properly resolve the generation of these waves. The vertical wavelengths of the gravity waves are larger than ~7 km, and therefore they are represented by at least 36 vertical grid points.

To ensure that the sensitivity of the modeled waves to horizontal resolution is not solely a product of the CHM, we also examined results from the WRF Model. Vertical velocity from simulations by the WRF Model with $\Delta X = 1.5$ km and $\Delta Z = 200$ m is shown in Fig. 3b. The WRF Model produces wave signatures in vertical velocity that are similar to those produced by the CHM. However, the horizontal wavelength of the waves is slightly smaller, and the amplitudes are larger.

To illustrate the sensitivity of the horizontal scale of the gravity waves to horizontal grid spacing, a set of horizontal power spectra for four different grid spacings are shown in Fig. 4. These spectra are calculated from vertical velocity at 15 km AGL in the CHM simulations with $\Delta X = 2$ km, 1 km, 500 m, and 125 m. The spectra are averaged from 2-min output over the first 3 h of each simulation. Each individual spectrum exhibits a rapid reduction in power at wavenumbers corresponding to wavelengths ~$8\Delta X$, and therefore we trun-

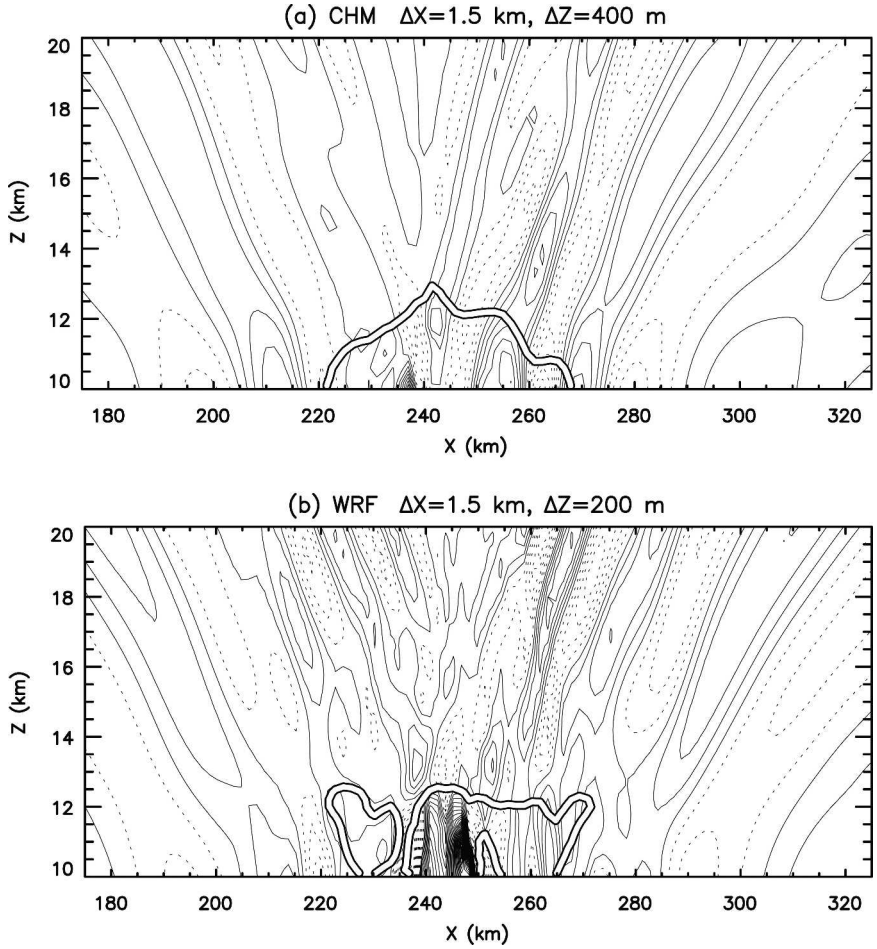

FIG. 3. Contours of vertical velocity at 60 min. The contour interval is 0.5 m s^{-1}, and negative values are dashed. The black-edged white line is the cloud water mixing ratio contour of 0.05 g kg^{-1}. Simulations are by (a) the CHM initialized with the WK sounding, with ΔX = 1.5 km and ΔZ = 400 m, and by (b) the WRF Model initialized with the WK sounding, with ΔX = 1.5 km and ΔZ = 200 m.

cated the spectra at wavenumbers that exceed $2\pi/8\Delta X$. The spectral analysis shows that for the two coarse simulations (ΔX = 2 km and 1 km), the strongest spectral peak occurs at wavenumbers corresponding to wavelengths $\sim 15\Delta X$. At higher resolutions, an absolute peak at $\sim 15\Delta X$ is not present, and the corresponding wavenumbers are in regions of relatively low spectral power. At wavenumbers above 0.0003 rad m^{-1}, the spectra for the 500- and 125-m simulations are similar, implying that the solutions have approximately converged. Thus, it appears that the coarse simulations have not reached numerical convergence, and artificially strong spectral peaks occur close to the limit of the model's resolution. A chi-square test, with 180 degrees of freedom (Jenkins and Watts 1968), shows that the $\sim 15\Delta X$ peaks of the 2- and 1-km simulations satisfy a 95% confidence test, whereas the spectra of the finer simulations do not have any peaks around $\sim 15\Delta X$ that satisfy the confidence test. Moreover, these $\sim 15\Delta X$ peaks in the 2- and 1-km simulations correspond to the visually obvious wavelength evident in contour plots of vertical velocity (such as Fig. 1b).

These peaks in the wave field at $\sim 15\Delta X$ in the 2- and 1-km simulations do not necessarily imply that numerical diffusion is strongly reducing power in the relatively long waves that are represented immediately to the right of $\sim 15\Delta X$ in Fig. 4. In fact, similar spectra through the middle of the cloud (not shown) exhibit strong power down to about $6–8\Delta X$, implying that numerical diffusion is not particularly strong between $\sim 8\Delta X$ and $\sim 15\Delta X$. Features in the spectra at $6–8\Delta X$ may not be effective gravity wave sources (see, e.g., Song et al. 2003), and therefore may not contribute to the wave spectrum measured aloft.

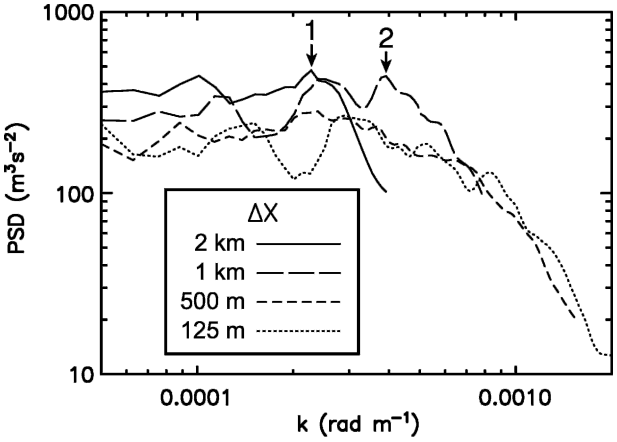

FIG. 4. The horizontal power spectra for the CHM simulations initialized with the WK sounding with $\Delta X = 2$ km, 1 km, 500 m, and 125 m. The spectra are calculated from the vertical velocity at 15 km, averaged for the 3 h of simulation, and shown truncated at wavenumbers greater than $2\pi/8\Delta X$. Arrows 1 and 2 mark the peaks at $\sim 15\Delta X$ for the 2- and 1-km simulations, respectively.

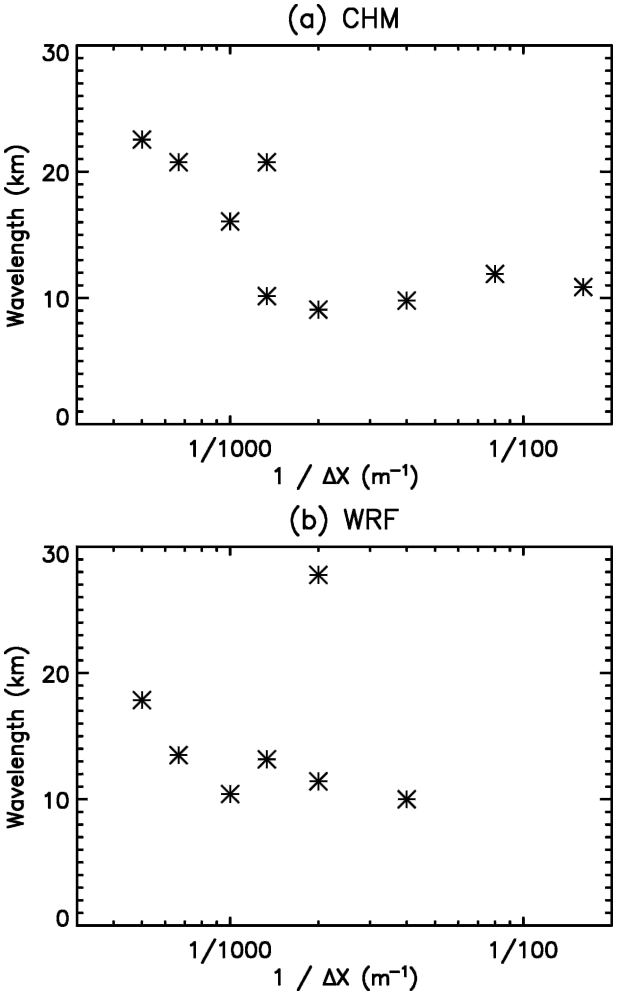

FIG. 5. The horizontal wavelengths that correspond to the peaks in the horizontal power spectra for frequencies between 0.007 and 0.015 rad s^{-1}, from simulations by (a) the CHM and (b) the WRF Model. All simulations were initialized with the WK sounding.

The focus of this study is on those high-frequency waves that are evident in the vertical velocity above the clouds, but the one-dimensional power spectra shown in Fig. 4 contain contributions from all frequencies, including low ones due to convective evolution, which may not be gravity waves. Therefore, in some cases these spectra contain no obvious peaks that correspond to the horizontal scales clearly evident in the vertical velocity.

To isolate the dominant horizontal wavelength of the high-frequency waves, we performed the following analysis. Two-dimensional (dimensions of frequency and horizontal wavenumber) spectra were constructed from the vertical velocity at 15 km AGL from 2-min output during the first 3 h of the simulations [similar to those spectra in the paper by Lane et al. (2003)]. The wavenumber spectra with frequencies between 0.007 and 0.015 rad s^{-1} (periods between 15 and 7 min) were combined to form one-dimensional power spectra, which we call the *filtered* power spectra. For each model simulation initialized with the WK sounding, the maxima of the filtered spectra are shown in Fig. 5. [Note that the analysis identifies peaks in the filtered spectra that appear anomalous for $\Delta X = 750$ m (CHM) and $\Delta X = 500$ m (WRF Model). For these two simulations, the filtered spectra possess two peaks of similar amplitude, which both satisfy a 95% confidence test, and the next most powerful peak in each filtered spectrum is also shown.]

Each model's simulation in Fig. 5 shows an obvious trend in the dominant horizontal wavelength of the high-frequency gravity waves. The coarsest simulations by the CHM have dominant high-frequency waves with wavelengths around 20 km. This dominant wavelength shrinks rapidly with grid spacing to ~10 km at $\Delta X = 500$ m. The dominant wavelength does not converge to a single value and varies by a few kilometers as the grid spacing is reduced further. This probably represents uncertainty in the analysis. The dominant wavelength of ~16 km for $\Delta X = 1$ km is consistent with those estimates made by Lane and Reeder (2001) using a three-dimensional model. The ~10 km wavelength identified in the finer simulations is larger than those identified by Lane et al. (2003) using a two-dimensional model at 50-m grid spacing. However, the analysis herein identifies the most powerful high-frequency gravity wave, so significant contributions can also exist from smaller and/or larger wavelengths.

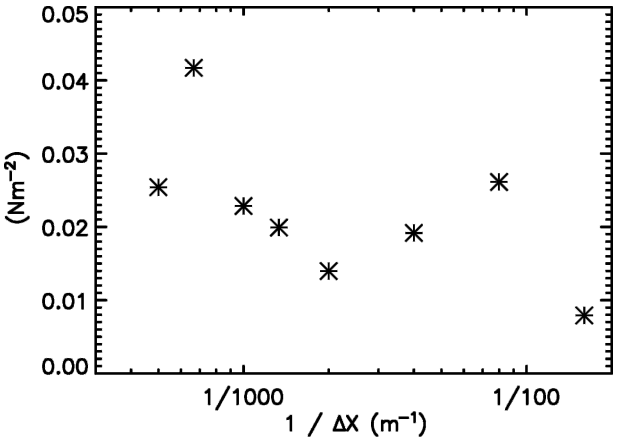

FIG. 6. Momentum flux at 25 km AGL for all CHM simulations initialized with the WK sounding. The momentum flux is calculated as an average over the central 250 km of the model domain, for the first 3 h of simulation.

The spectral analysis considered above incorporated the rapid start-up phase of the convection during the first hour of each simulation. To test whether this inclusion significantly affects our results, we also calculated a number of spectra for the CHM simulations over only their last 2 h. The test produced results that were qualitatively similar to those from the full simulations, so we conclude that the rapid start-up phase of the convection did not significantly affect the spectra. The reason we included the full simulations in our formal spectral analyses is that each convective system evolved at a slightly different pace, so including each simulation's first hour insured the most consistent comparisons.

The WRF Model appears to converge to the ~10 km wavelength at larger grid spacings than the CHM does. At grid spacings greater than 1 km, the solutions undergo a significant change with resolution, but this change is not as large as those in simulations by the CHM. The WRF Model's more rapid convergence, as well as the increased amplitude of the waves mentioned earlier, is probably due to the model's higher-order spatial differencing and to the implicit filtering employed. This result is consistent with other research that suggests that the WRF Model's high-order numerics results in less dissipation and more detail at high wavenumbers than is present in other models that use lower-order numerics (e.g., Baldwin and Wandishin 2002; Skamarock 2004).

We calculated the momentum flux for all of the CHM simulations initialized with the WK sounding (Fig. 6). Vertical profiles of momentum flux were calculated by averaging $\rho u'w'$ over the central 250 km of the model domain for the first 3 h of simulation (wherein ρ is density, and u' and w' are the deviations of horizontal and vertical velocity from their horizontal, domainwide averages, respectively). In the WK sounding there is no background vertical wind shear in the stratosphere, so almost the entire spectrum of waves can propagate vertically and therefore each profile of momentum flux in the stratosphere is approximately constant with altitude (a layer we call the *free stratosphere* for the purposes of this paper). The specific values of this momentum flux vary with resolution because wave spectra vary with resolution. However, the trend in momentum flux (Fig. 6) is less systematic than is the trend in horizontal wavelength (Fig. 5). It seems that in unsheared flow, momentum flux is not as strongly coupled to horizontal grid resolution as is the horizontal wavelength of the dominant gravity waves.

b. Sheared flow in the upper troposphere and lower stratosphere

In the previous section, spectral analyses showed that the wavelengths of high-frequency gravity waves are highly sensitive to model grid spacing. A decrease of the CHM's grid spacing from O(1 km) to O(100 m) reduced the dominant wavelength by about a factor of one-half, from 20 to 10 km. This reduction, although seemingly minor, can have important implications for wave propagation. As an example, consider the simplified criterion for vertical gravity wave propagation:

$$0 < |\omega - Uk| < N,$$

wherein ω is frequency, U is background wind speed, k is horizontal wavenumber, N is the Brunt–Väisälä frequency, and $\omega - Uk$ is known as the intrinsic frequency. For high-frequency waves with ω close to N, and a large wavenumber, k, a small change in background wind speed can cause the wave to be trapped ($|\omega - Uk| = N$). Also, for a given frequency, waves with shorter wavelengths are more susceptible to dissipation at a critical level ($|\omega - Uk| = 0$) than are waves with longer wavelengths (Lane and Clark 2002).

Two simulations initialized with the BIS sounding are shown in Fig. 7 for (a) $\Delta X = 1.5$ km and (b) $\Delta X = 62.5$ m. Most of the phase lines of the waves in (a) are at some angle to the vertical, and their amplitudes are either constant or increasing with altitude. These are vertically propagating waves. In (b) however, most of the phase lines of the waves are vertical, and in general the amplitudes of the waves decrease considerably with altitude. These waves are vertically trapped. *A simple change in grid spacing converted vertically propagating waves to vertically trapped waves.*

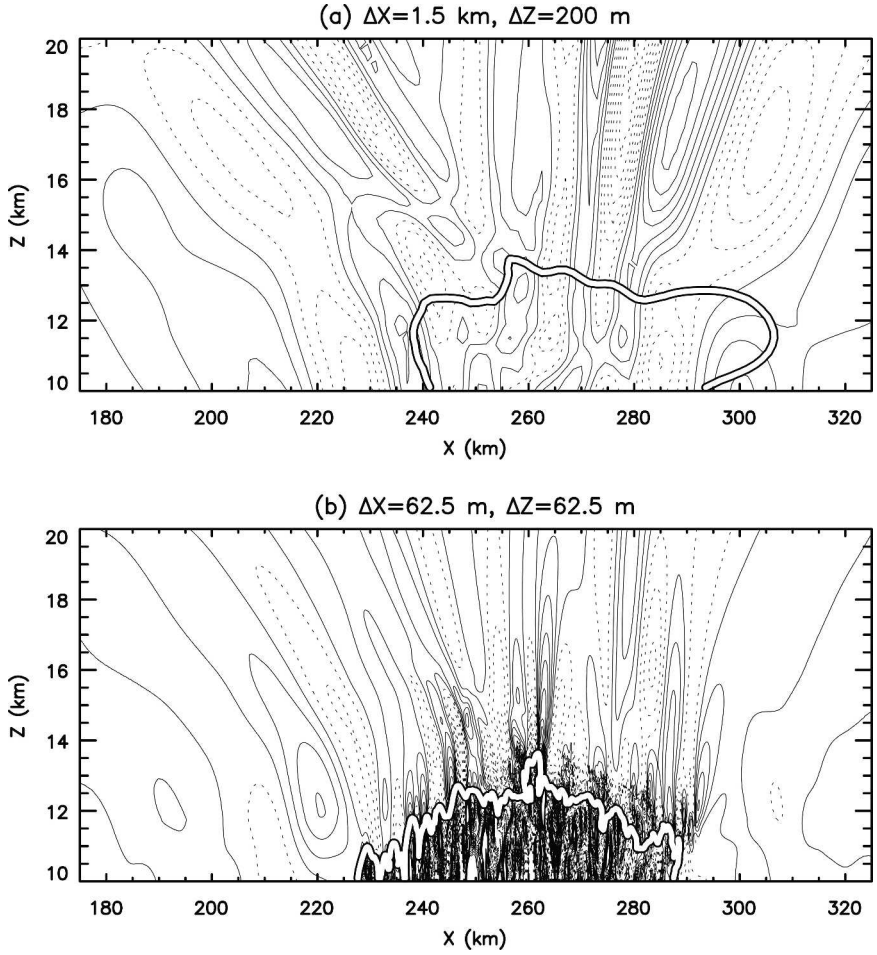

FIG. 7. Contours of vertical velocity at 60 min into simulations by the CHM, initialized with the BIS sounding. Grid spacings are (a) $\Delta X = 1.5$ km and $\Delta Z = 200$ m, and (b) $\Delta X = 62.5$ m and $\Delta Z = 62.5$ m. The contour interval is 0.5 m s^{-1} and negative values are dashed. In (a) and (b), the black-edged white line is the cloud water mixing ratio contour of 0.05 g kg^{-1}.

To further illustrate the effects of horizontal resolution on the spectra of gravity waves in sheared conditions, consider two-dimensional (dimensions of frequency and horizontal wavenumber) power spectra for two cases that clearly identify the processes at work, with $\Delta X = 2$ km and $\Delta X = 125$ m (Fig. 8). These spectra were calculated using the vertical velocity at 15 km AGL, over the central 250 km of the model domain, for 180 min (at 2-min intervals). Figure 8 shows the square of the absolute value of the amplitude spectra (i.e., the power) averaged over nine adjacent frequency/wavenumber bins. These spectra show the ground-based frequency, but because the background wind speed at 15 km AGL is approximately zero, this frequency is also the intrinsic frequency of the gravity waves. If frequency is assumed to be nonnegative, positive horizontal wavenumbers represent waves with positive horizontal phase velocities, and negative horizontal wavenumbers represent waves with negative phase velocities. The spectrum of the 2-km simulation (Fig. 8a) shows its strongest peaks at horizontal wavenumbers less than 0.4×10^{-3} rad m^{-1} (wavelengths greater than 15 km), and intrinsic frequencies less than about 12×10^{-3} rad s^{-1}. On the other hand, the spectrum of the 125-m simulation (Fig. 8b) shows a substantial reduction in power at low wavenumbers and frequencies, and the strongest peak in the spectrum is at a wavenumber equal to 0.6×10^{-3} rad m^{-1} (wavelength of 10 km) and a frequency equal to 20×10^{-3} rad s^{-1}. The finer simulation has its strongest peak at a higher wavenumber than the coarser simulation. This increase in power at higher wavenumbers is at the expense of the power at lower wavenumbers in the coarser simulation; both spectra have similar maxima (Fig. 8a: 2.0×10^{-3} m^2 s^{-2}; Fig. 8b: 2.6×10^{-3} m^2 s^{-2}). Also, both wave fields have similar average values of kinetic en-

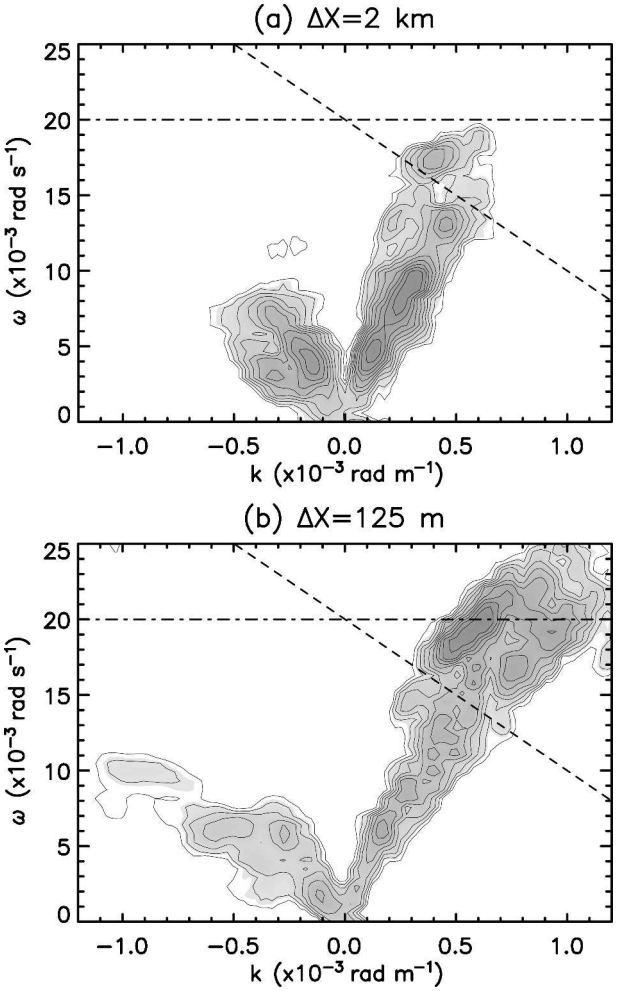

FIG. 8. Two-dimensional (k, ω) power spectra of vertical velocity at 15-km altitude for CHM simulations initialized with the BIS sounding. Grid spacings are (a) $\Delta X = 2$ km and $\Delta Z = 200$ m, and (b) $\Delta X = 125$ m and $\Delta Z = 100$ m. The spectra are normalized by their maximum value: (a) 2.0×10^{-3} m^2 s^{-2} and (b) 2.6×10^{-3} m^2 s^{-2}. Only the largest two orders of magnitude are contoured (in 11 logarithmic contours 10^{-2}, $10^{-1.8}$, . . . , $10^{-0.2}$, 1). Also shown are the *trapping lines* (see text) at 15 km (dotted–dashed) and 20 km (dashed).

ergy per unit mass[1] of 3.58 m^2 s^{-2} for the 2-km simulation and 3.88 m^2 s^{-2} for the 125-m simulation.

As discussed by Lane et al. (2003), through Doppler shifting from their source reference frame, gravity waves with higher horizontal wavenumbers can attain a larger intrinsic frequency more easily than can waves with lower horizontal wavenumber. This is clearly illustrated in Fig. 8. As mentioned earlier, a wave will become vertically trapped if its intrinsic frequency exceeds the Brunt–Väisälä frequency, which in this case is approximately 0.02 rad s^{-1} in the stratosphere. Frequencies in each spectrum at which the waves become trapped are marked in Fig. 8; waves with frequencies greater than these *trapping lines* (see Lane and Clark 2002) are vertically trapped. Trapping lines are shown for 15 km AGL ($\omega = N = 0.02$) and 20 km AGL ($\omega = N - 10k$, where -10 m s^{-1} is the wind speed at 20 km). Therefore, at 15 km AGL the strongest spectral peak in the finer simulation is close to being vertically trapped, whereas the strongest spectral peaks in the coarser simulation are well below the trapping line and are able to propagate vertically. At 20 km, the strongest waves in the coarser simulation can still propagate vertically, but those in the finer simulation cannot.

Vertically propagating waves generally cause a vertical flux of horizontal momentum, but vertically trapped waves do not. It can be shown, based on mass continuity, that the momentum flux, $\rho u'w'$, varies like $A_w m/k$, wherein A_w is the vertical velocity amplitude, and m is the vertical wavenumber. Thus, as a wave approaches being trapped, m tends to zero, and so does the momentum flux. Therefore, it seems reasonable to assume that in cases where a change in resolution causes the modeled waves to undergo the transition from vertically propagating to vertically trapped, the increase in resolution may also substantially reduce momentum flux.

For each of the simulations initialized with the BIS sounding, to create vertical profiles the momentum flux is averaged over the central 250 km of the model domain for 2-min output during the first 3 h of the simulation. A subset of these vertical profiles is shown in Fig. 9. All profiles show a similar shape, with negative momentum flux near cloud top changing to positive momentum flux at higher altitudes. Above about 20 km AGL, the momentum flux is almost constant with altitude. There is significant variation among the individual profiles in the region of vertical momentum-flux divergence (<20 km AGL). The amplitudes of momentum flux above the region of momentum-flux divergence is highly sensitive to resolution. Momentum flux at 25 km AGL for all of the CHM simulations initialized with the BIS sounding is shown in Fig. 10. This free-stratospheric momentum flux represents the potential influence of the gravity waves on the upper atmosphere. The momentum flux decreases significantly with grid spacing. This reduction is because power shifts from waves with long wavelengths to waves with short wavelengths, and the latter are trapped and do not transport momentum. The wave spectrum is cer-

[1] The kinetic energy per unit mass is $(u'^2 + w'^2)/2$; the average is calculated over the central 250 km of the domain at 15 km AGL, for 180 min at 2-min intervals.

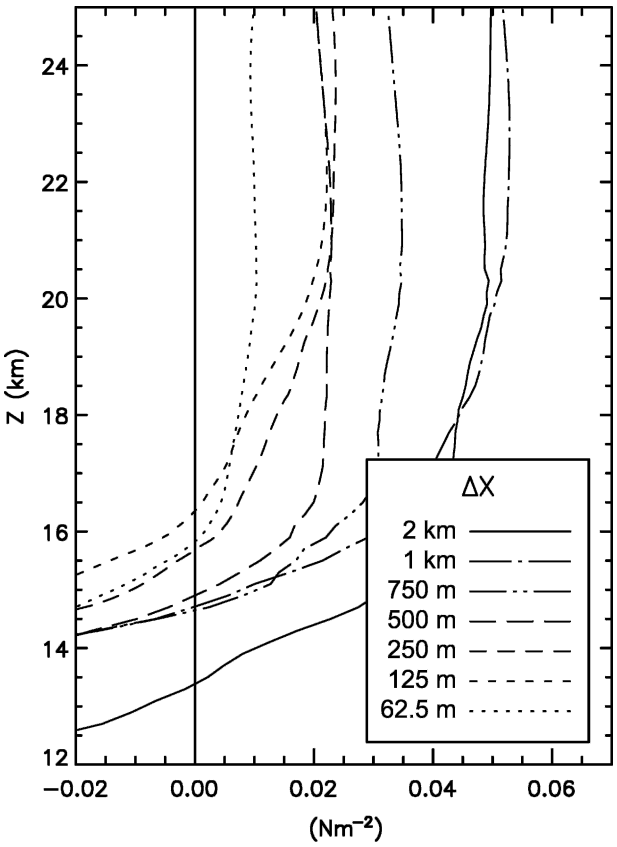

FIG. 9. Momentum flux profiles for a subset of the CHM simulations initialized with the BIS sounding. The momentum flux is calculated as an average over the central 250 km of the model domain, for the first 3 h of simulation.

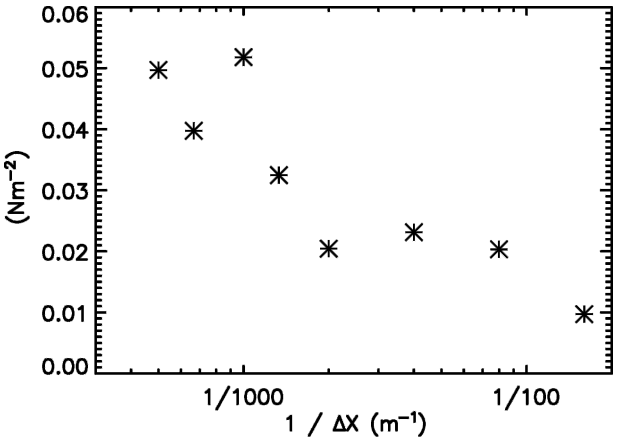

FIG. 10. Momentum flux at 25 km AGL for all CHM simulations initialized with the BIS sounding. The momentum flux is calculated as an average over the central 250 km of the model domain, for the first 3 h of simulation.

tainly not monochromatic, and therefore some power remains in those wavenumbers that can propagate vertically, accounting for the nonzero momentum flux aloft that is almost constant with altitude. Momentum flux in the free stratosphere does not show the same apparent convergence as the dominant wavelength does (Fig. 5) and it continues to decrease with grid spacing. (Momentum flux in Fig. 10 should not be directly compared to that in Fig. 6, because of the different vertical wind shears.)

To provide further detail, we constructed a spectral representation of the momentum flux. These spectra were calculated by multiplying the density by the real part of the cospectra of u' and w', using the same horizontal and temporal domains that were used to calculate Fig. 9. At each altitude, the sum of the momentum flux spectral components is equal to the simple average of $\rho u'w'$ shown in Fig. 9. For each altitude, the cospectra were used to separate the positive and negative contributions of the flux; these components and their total are shown in Fig. 11 for two cases. This figure shows that in both cases, the total momentum flux comprises a positive and negative contribution; in the free stratosphere the positive contribution is about 3 times the magnitude of the negative contribution, resulting in positive total momentum flux. In both cases, each cospectrum shows that these contributions are derived mostly from the low-frequency, low-wavenumber waves seen in Fig. 8. The positive and negative momentum flux contributions shrink with decreasing grid spacing, resulting in a reduction in the

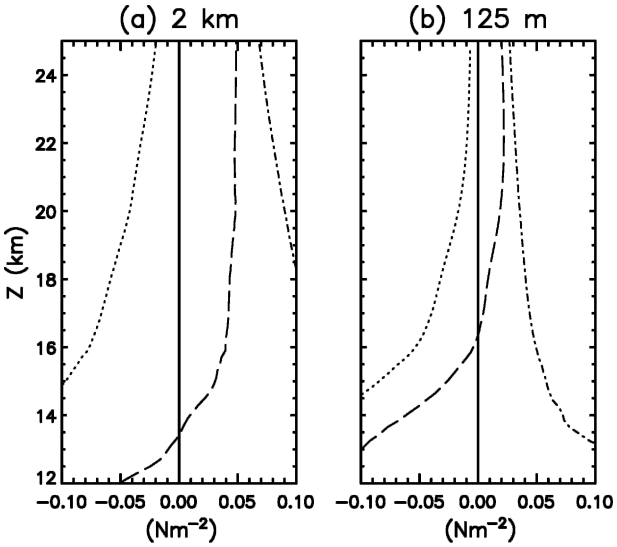

FIG. 11. Momentum flux profiles for CHM simulations initialized with the BIS sounding with (a) $\Delta X = 2$ km and (b) $\Delta X = 125$ m. Using the cospectra, the momentum flux was separated into the negative contribution (dotted) and the positive contribution (dotted–dashed); the total momentum flux is the dashed line.

total momentum flux. This reduction in the (positive and negative) momentum flux is due mostly to the reduction in the power of the waves that have a lower wavenumber and lower intrinsic frequency. The higher-wavenumber waves that dominate the spectrum in Fig. 8b do not contribute to the momentum flux because they are trapped.

The trend in momentum flux in Fig. 10 is not due to a reduction in convective intensity with increasing resolution. We verified this point by approximating convective intensity as the average of the square of the vertical velocity, $\langle w^2 \rangle$, calculated over the central 100 km of the model domain at 10 km AGL for the first 3 h of simulations. This measure represents the strength of convective updrafts and downdrafts that influence the upper troposphere, tropopause, and lower stratosphere—that is, the region of wave excitation. For simulations initialized with the BIS sounding, $\langle w^2 \rangle$ generally increased with model resolution from $\sim$6 m^2 s^{-2} (ΔX = 2 km) to $\sim$10 m^2 s^{-2} (ΔX = 62.5 m).

4. Summary and final comments

We used the Clark–Hall Model (CHM) to demonstrate that simulated, high-frequency gravity waves generated by mesoscale convection are highly sensitive to horizontal grid spacing. We then tested our results' sensitivity to vertical resolution and verified that switching to the Weather Research and Forecasting (WRF) Model did not significantly affect our primary conclusions. Results from the two-dimensional simulations by both models can be used as a guide for future three-dimensional modeling studies.

The key conclusion of this study is that coarse simulations by cloud-resolving models poorly represent the details of convective updrafts and the gravity waves they generate. The horizontal scale of the updrafts is tied to the smallest resolvable scale of the model. Such simulations may produce dominant gravity waves that *seem* to be adequately resolved, but the spectra of these waves are not robust. At higher resolutions, convective updrafts in clouds, and hence wave sources, are better represented, so the characteristics of the updrafts and mixing are determined by the internal dynamics of the modeled cloud and are not dominated by numerical effects. In such cases, the response and the details of the wave propagation characteristics are more reliable (i.e., the gravity waves have more robust spectra).

In simulations by the CHM with no shear above the lower troposphere, the coarsest horizontal grid spacing (2 km) led to dominant wavelengths of $\sim$20 km, but the finest grid spacing (62.5 m) led to dominant wavelengths of $\sim$10 km. The dominant wavelength decreased with decreasing grid spacing until $\Delta X \sim$500 m; at finer grids the dominant horizontal wavelength reached approximate convergence. Trends in the WRF Model, which uses higher-order finite-difference schemes, were grossly similar, except that simulations by the WRF Model resembled simulations by the CHM with finer grid spacing. We conclude that higher-order numerics proved most valuable at large grid spacings, but not necessarily at the smallest grid spacings we tested, because by then the gravity wave properties had already converged.

The coarse simulations produced artificially strong peaks in the power spectra of vertical velocity at wavelengths $\sim 15\Delta X$. As we increased resolution, the power in the spectral peaks was reduced, and power shifted to higher wavenumbers. It is these higher wavenumbers that dominate the spectrum of high-frequency waves. Waves seen in the coarse simulations played a less important role once the solutions converged. In the absence of wind shear almost the entire spectrum of gravity waves was able to propagate vertically, and therefore contributed to the momentum flux. Therefore, in unsheared flow the changes in the wave spectrum only weakly influenced the momentum flux, which did not exhibit a clear, regular trend with horizontal grid spacing.

As shown in previous studies (e.g., Lane and Clark 2002), short-wavelength gravity waves are more readily filtered by wind shear through trapping and dissipation at a critical level. To test the effect of the gravity waves whose wavelengths were reduced by increased resolution, we performed another series of simulations using a real sounding with moderate, lower-stratospheric, vertical wind shear. The coarsest of these simulations are dominated by vertically propagating waves, the finest are dominated by vertically trapped waves. As a result, the *free-stratospheric* momentum flux is lower for the most resolved simulations.

The results in this paper suggest that previous studies that used O(1 km) grid spacing may have overestimated the horizontal wavelength of the highest-frequency gravity waves generated by deep mesoscale convection. Overestimations of wavelength can lead to overestimations of momentum flux in cases with wind shear above cloud top. This adds uncertainty to previous estimates of the relative role of convectively generated gravity waves in forcing the quasi-biennial oscillation (QBO). Moreover, the extent to which the converged spectrum of gravity waves is filtered by the background wind suggests that high-frequency gravity waves are more confined to the stratosphere than previously thought, and they may contribute relatively little to the momentum budget of the mesosphere. Our results also suggest

that using explicit estimates of gravity wave momentum flux from the relatively coarse cloud-resolving elements within superparameterizations for GCMs (Randall et al. 2003) may not be entirely successful. However, such superparameterizations promise vast improvement in representing many aggregate effects of convectively generated gravity waves, which probably outweighs the uncertainty caused by the coarseness of the cloud-resolving elements.

In conclusion, we recommend that estimates of momentum flux and gravity wave drag from coarse cloud-scale models be interpreted cautiously because of the relatively large sensitivity to model resolution. Rigorous sensitivity studies are crucial to determine the necessary resolution, which may be case and/or model dependent. Finally, our simulations are two-dimensional; the details of wave dissipation and dispersion are different in three dimensions, and an in-depth three-dimensional study is a topic for future research.

Acknowledgments. This study has benefited from the authors' conversations with Joan Alexander, Jadwiga Beres, George Bryan, Dale Durran, Rod Frehlich, Jim Holton, Michael Reeder, and Fuqing Zhang. We also thank Robert Fovell, Bob Sharman, and two anonymous reviewers for their comments on an earlier version of the manuscript.

REFERENCES

Alexander, M. J., and J. R. Holton, 1997: A model study of zonal forcing in the equatorial stratosphere by convectively induced gravity waves. *J. Atmos. Sci.,* **54,** 408–419.

——, J. H. Beres, and L. Pfister, 2000: Tropical stratospheric gravity wave activity and relationships to clouds. *J. Geophys. Res.,* **105,** 22 299–22 309.

Baldwin, M. E., and M. S. Wandishin, 2002: Determining the resolved spatial scales of ETA Model precipitation forecasts. Preprints, *19th Conf. on Weather Analysis and Forecasting and the 15th Conf. on Numerical Weather Prediction,* San Antonio, TX, Amer. Meteor. Soc., 85–88.

Beres, J. H., M. J. Alexander, and J. R. Holton, 2002: Effects of tropospheric wind shear on the spectrum of convectively generated gravity waves. *J. Atmos. Sci.,* **59,** 1805–1824.

——, ——, and ——, 2004: A method of specifying the gravity wave spectrum above convection based on latent heating properties and background wind. *J. Atmos. Sci.,* **61,** 324–337.

Bryan, G. H., J. C. Wyngaard, and J. M. Fritsch, 2003: Resolution requirements for the simulation of deep moist convection. *Mon. Wea. Rev.,* **131,** 2394–2416.

Clark, T. L., 1977: A small-scale dynamic model using a terrain-following coordinate transformation. *J. Comput. Phys.,* **24,** 186–215.

——, W. D. Hall, and J. L. Coen, 1996: Source code documentation for the Clark–Hall cloud-scale model: Code version G3CH01. NCAR Tech. Note NCAR/TN-426+STR, 137 pp.

Fovell, R., D. Durran, and J. R. Holton, 1992: Numerical simulations of convectively generated stratospheric gravity waves. *J. Atmos. Sci.,* **49,** 1427–1442.

Fritts, D. C., and M. J. Alexander, 2003: Gravity wave dynamics and effects in the middle atmosphere. *Rev. Geophys.,* **41,** 1003, doi:10.1029/2001RG000106.

Holton, J. R., J. H. Beres, and X. Zhou, 2002: On the vertical scale of gravity waves excited by localized thermal forcing. *J. Atmos. Sci.,* **59,** 2019–2023.

Jenkins, G. M., and D. G. Watts, 1968: *Spectral Analysis and Its Applications.* Holden-Day, 525 pp.

Kershaw, R., 1995: Parametrization of momentum transport by convectively generated gravity waves. *Quart. J. Roy. Meteor. Soc.,* **121,** 1023–1040.

Kessler, E., 1969: *On the Distribution and Continuity of Water Substance in Atmospheric Circulations. Meteor. Monogr.,* No. 32, Amer. Meteor. Soc., 84 pp.

Koenig, L. R., and F. W. Murray, 1976: Ice-bearing cumulus cloud evolution: Numerical simulation and general comparison against observations. *J. Appl. Meteor.,* **15,** 747–762.

Lane, T. P., and M. J. Reeder, 2001: Modelling the generation of gravity waves by a maritime continent thunderstorm. *Quart. J. Roy. Meteor. Soc.,* **127,** 2705–2724.

——, and T. L. Clark, 2002: Gravity waves generated by the dry convective boundary layer: Two-dimensional scale selection and boundary layer feedback. *Quart. J. Roy. Meteor. Soc.,* **128,** 1543–1570.

——, R. D. Sharman, T. L. Clark, and H.-M. Hsu, 2003: An investigation of turbulence generation mechanisms above deep convection. *J. Atmos. Sci.,* **60,** 1297–1321.

Lin, Y. L., R. D. Farley, and H. D. Orville, 1983: Bulk parameterization of the snow field in a cloud model. *J. Climate Appl. Meteor.,* **22,** 1065–1092.

Pfister, L., S. Scott, M. Loewenstein, S. Bowen, and M. Legg, 1993: Mesoscale disturbances in the tropical stratosphere excited by convection: Observations and effects on the stratospheric momentum budget. *J. Atmos. Sci.,* **50,** 1058–1075.

Piani, C., D. Durran, M. J. Alexander, and J. R. Holton, 2000: A numerical study of three-dimensional gravity waves triggered by deep tropical convection and their role in the dynamics of the QBO. *J. Atmos. Sci.,* **57,** 3689–3702.

Randall, D., M. Khairoutdinov, A. Arakawa, and W. Grabowski, 2003: Breaking the cloud parameterization deadlock. *Bull. Amer. Meteor. Soc.,* **84,** 1547–1564.

Skamarock, W. C., 2004: Evaluating mesoscale NWP models using kinetic energy spectra. *Mon. Wea. Rev.,* **132,** 3019–3032.

——, J. B. Klemp, and J. Dudhia, 2001: Prototypes for the WRF (Weather Research and Forecasting) Model. Preprints, *Ninth Conf. on Mesoscale Processes,* Fort Lauderdale, FL, Amer. Meteor. Soc., J11–J15.

Song, I.-S., H.-Y. Chun, and T. P. Lane, 2003: Generation mechanisms of convectively forced internal gravity waves and their propagation to the stratosphere. *J. Atmos. Sci.,* **60,** 1960–1980.

Weisman, M. L., and J. B. Klemp, 1982: The dependence of numerically simulated convective systems on vertical wind shear and buoyancy. *Mon. Wea. Rev.,* **110,** 504–520.

Wicker, L. J., and W. C. Skamarock, 2002: Time splitting methods for elastic models using forward time schemes. *Mon. Wea. Rev.,* **130,** 2088–2097.

AMS Copyright Notice